RESEARCH ARTICLE

INVESTIGATION OF FLOW CHARACTERISTICS FOR A MULTI-STAGE TESLA VALVE AT LAMINAR AND TURBULENT FLOW CONDITIONS

Ahmet Alper YONTAR[1]*, Duygu SOFUOĞLU[2], Hüseyin DEĞİRMENCİ[3], Mert Şevket BİÇER[4], Tahir AYAZ[5]

[1]Tarsus University, Mechanical Engineering Department Faculty of Engineering, Mersin, aayontar@tarsus.edu.tr, ORCID: 0000-0002-5453-5137
[2]Tarsus University, Manufacturing Engineering Department Graduate Education Institute, Mersin, duygu_sofuoglu@tarsus.edu.tr, ORCID: 0000-0001-5522-7331
[3]Tarsus University, Automotive Engineering Department Graduate Education Institute, Mersin, huseyin_degirmenci@tarsus.edu.tr, ORCID: 0000-0001-7585-8907
[4]Tarsus University, Mechanical Engineering Department Graduate Education Institute, Mersin, mert_bicer@tarsus.edu.tr, ORCID: 0000-0002-9215-6787
[5]Tarsus University, Automotive Engineering Department Graduate Education Institute, Mersin, tahir_ayaz@tarsus.edu.tr, ORCID: 0000-0002-1291-987X

ABSTRACT

Tesla valve is a passive type check valve that empowers flow in one direction without moving parts used for flow control in mini or microchannel systems. It is a system that can be used for a long time with low fatigue and low wear due to the lack of moving parts in its structure. Besides the cost of production is cheap due to its simple geometry. Also, the Tesla valve differs from all other valves with these features. Allowing or preventing the movement of the fluid is due to the specific design of the profiles inside the valve. In addition, the fluid that encounters obstacles at high velocities continues on its way by gaining thermodynamic properties. The efficiency of the Tesla valve is measured by diodicity, which can be managed by small losses due to direction during forward or reverse flows, primarily along with the flow inlet speed and flow line design. In this study, the variation of the velocities of methane gas in the specially designed Tesla valve has been investigated in detail via numerical analysis. Tesla valve structure with eleven flow control segments was used in the analysis. Moreover, the fluid motion behaviors in both directions were investigated for laminar and turbulent velocities. As a result of the study, the turbulence kinetic energy change and diodicity were determined for methane use in the Tesla valve. Also, different characteristic features of laminar and turbulent flow have been revealed in the tesla valve.

Keywords: *Tesla Valve, Methane, Computational Fluid Dynamics, Diodicity, Turbulence Kinetic Energy.*

1. INTRODUCTION

Check valves without moving parts provide flow control in mini-micro channels [1-5] and the valves have a pressure drop based on the direction. As a consequence of the properties, the trend determines the progress of the flow direction. Small pressure losses occur depending on the flow direction owing

to their unique designs. Current flow in forwarding and reverse direction acquires diode feature to the fluid. Check valves have features that can be easily scaled and manufactured by separating them from micro-pumps containing moving parts. Besides, check valves can be used with colloidal suspensions. Check valves under the favor of these advantages; It has been used frequently in biotechnological devices, microelectromechanical systems, analytical chemistry, health, and engineering applications [1].

The Tesla valve was invented by Nikola Tesla, as it is well known. The Tesla valve was shown in Figure 1 consists of stationary parts that allow flow with low resistance in one direction but create high resistance to flow on the reverse. It is called reverse flow to the stream direction with high resistance and forward flow to the stream direction with low resistance. This difference in flow resistance causes a continuous directional flow velocity in the forward direction in oscillatory flows. The efficiency of a Tesla valve at constant velocities is measured by diodicity, which is the ratio of the pressure difference in the reverse and forward flow directions. The efficiency is frequently expressed as diodecity, which is the ratio of pressure drops for the same flow velocity. Small pressure losses in the Tesla valve; flow splitting is due to sudden expansion and jet impingement. The equation that can be seen below characterizes the ability to pass flow in the forward direction while inhibiting flow in the reverse direction. The differential pressure loss that forms the diodicity of a Tesla valve is due to inertial and viscous force.

$$Di = \left(\frac{\Delta P_r}{\Delta P_f}\right)_Q \qquad\qquad (1)$$

ΔP_f represents the forward flow drop for flow rate Q and ΔP_r means that the pressure drop of the reverse flow. The literature on the use of Tesla valve, there are studies in various content and approaches. Some of these studies are briefly summarized in the following section.

Truong and Nguyen [6] conducted a numerical study to obtain the optimum geometry in the Tesla valve. They have been analyzed two-dimensional (2D) geometries with different flow rates and different channel angles (00-800) for the case of Reynolds number (Re <1000). As a result of the study, it was determined that the most suitable design is the Tesla valve with T45-R geometry with a canal angle of 450 in the range of 100 <Re <600.

Forster et al. [7] studied the efficiency of the diffuser valve and Tesla valve employing a piezo-operated pump. In the present study, they have been conducted an experimental study to develop efficient non-moving split valves and to provide optimum Tesla valve geometry. Consequently, it has been determined that Tesla valves have higher diodes than diffuser check valves. It has been found that the diodicity increases linearly with the flow rate when the Re number is below 300 for the T45-R valve.

Zhang et al. [8] investigated the relationship between diodicity, pressure drop, and flow rate in T45-R valve in three dimensions (3D) at Re = 2000. It has been observed that it gives maximum diodicity in low Re (Re <500) numbers. According to the results obtained for the same hydraulic diameter, valves having a higher aspect ratio have been found that better performance is obtained.

Gamboa et al. [9] examined the Tesla-type valve for micro pump applications with six independent and dimensionless parameters. They have been benefited from 2D numerical simulations in their

optimization studies. As a result of the study, it has been determined that the optimized design provides 25% higher diodicity in the range of 0-2000 Reynolds number compared to the commonly used Tesla-type valve shape. The resulting valve was adopted as the Gamboa, Marris, and Forster (GMF) Tesla valve.

Thompson et al. [10] investigated laminar and turbulent flow regimes up to Re = 2000 using 3D CFD in Tesla valve at inlet Reynolds numbers. It was based on the RANS-based flow modeling approach used to measure diodicity, various models including k-ε, k-ω, and SST k-ω models were used in the study. It has been determined that the k-ω model and SST k-ω models perform more accurate simulations than laminar two-dimensional CFD analysis for the case where Re> 500 is in the Tesla valve. It has been found that the k-ω model and SST k-ω models perform more accurate simulations compared to the laminar two-dimensional CFD analysis for the situation where there is Re>500 in the Tesla valve. The k-ω model has been found to provide the best performance and show 6% maximum relative error with available experimental data for up to Re = 1500.

Mohammadzadeh et al. [11] numerically investigated the effect of Reynolds number and Tesla valve stage on diodicity. The study was carried out in 2D and the results of the wide-angle multistage tesla valve (MSTV) and the diffuser type no-moving parts valve (NMPV) were compared. They have been found that the diodeicity of wide-angle MSTV is superior to diffuser type NMPV in high Reynolds numbers (Re> 200), and that the diodety of low Reynolds numbers is lower than NMPV. Besides, it was observed that the diodicity increased in direct proportion to the Tesla valve stage at the Re> 50.

Porwal et al. [12] examined the effect of different stages of the Tesla valve on flow properties and thermal improvement on CFD in three dimensions. They have been investigated in the simulation results that Tesla valve design can achieve efficiency in terms of Nusselt number, Darcy friction factor, diodicity, thermal diodicity. They have been monitored that the heat transfer increase with the number of stages in the reverse flow Tesla valve.

Thompson et al. [13] performed three-dimensional analyzes to examine the effect of Tesla valve stage on diodicity under laminar flow conditions. In the analyzes, the effect of the parameters of valve stage (up to 20), valve distance and Reynolds number (up to Re = 200) on diodicity was investigated. Consequently, it was determined that the diodicity was directly proportional to the number of Re and the number of stages and inversely proportional to the valve distance. It has been observed that the number of valves and the distance between the valves have little effect on the diodicity when the Re number is below 50.

Bardel [14] investigated experimentally and numerically the effect of different Tesla valve designs on diodicity at low Reynolds numbers. It has been found to be dependent on viscous forces, laminar flow of different location and size, recirculating flow mechanisms for the diodicity mechanism in Tesla valve. The results were gained from 2D numerical studies have been confirmed by experimental results.

Qian et al. [15] studied the flow of Al_2O_3-water nano-fluid through a micro-scale T45-R type Tesla valve numerically. The effects of nano-liquid flow rate, flow percentage, pressure drop in forwarding and backward flows, diodicity, temperature, and nanoparticle volume fraction on Tesla valve were investigated. They have been detected that nanofluids flowed towards the straight channel of the bifurcated section in forwarding flow and towards the arc channel in the opposite direction. It was determined that the diodicity changes linearly with the flow rate.

Jin et al. [16] quantified the use of Tesla valves in hydrogen fuel cell electric vehicles. They have been investigated a wide range of velocities using parameters such as hydraulic diameter, valve angle and radius of the inner curve to increase the pressure drop in the Tesla valve. It has been detected that the pressure drop decreases with increasing hydraulic diameter and increases with large velocity inputs. It has been observed with a numerical study that a multi-stage Tesla valve is needed to ensure sufficient pressure drop.

Wang et al. [17] made a series of numerical studies to optimize the design of new type Tesla valve micro-mixers. It was determined that a three-unit Tesla type micro mixer provides high flow mixing performance and observed that the optimal geometry provides a low pressure drop over the Tesla type micro mixer arrangement.

Although there are few studies conducted with Tesla valve in the literature, the working range has been limited. In this study, the behavior of methane fuel delivery velocity in the flow lines of a specially designed Tesla valve is examined in detail via the two-dimensional (2D) computational fluid dynamics (CFD) method.

2. METHODOLOGY

The effects of gas fluid delivery at different velocities in an eleven-wing Tesla valve with a low angle configuration were studied via 2D-CFD modeling in this study. The motion attitude of methane fuel was investigated between 1 m/s - 10 m/s in reverse and forward flows. The geometric design of the Tesla valve is shown in Figure 1.
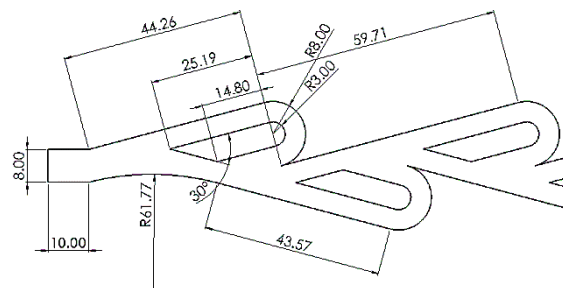
Figure 1. Tesla valve geometry.

As shown in Figure 2 that 10 lines other than the inlet and outlet line points were determined and evaluated for investigating the turbulence kinetic energy changes inside the Tesla valve. The lines were taken from the distance before 2 mm from the start of the point where the flow separates according to the reverse flow.
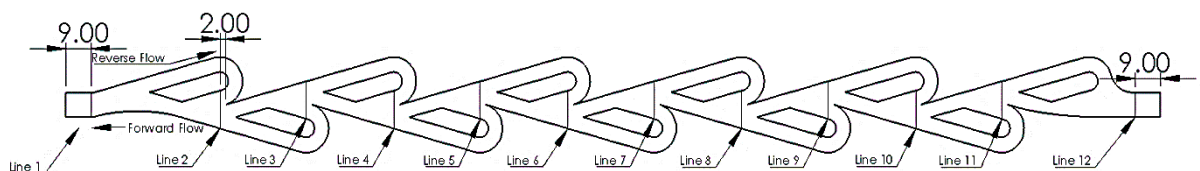

Figure 2. The positions of the lines.

Here, a very important detail should be taken into consideration while analyzing the study data. These are the flow from line 12 to line 1 in the forward flow where the reverse flow flows from line 1 to line 12.

$$Re_i = \frac{\rho u_i D_H}{\mu} \tag{2}$$

The Reynolds number is a unitless number that informant about the state of the fluid and it is described as the ratio of the inertia forces of the fluid to the viscosity forces. In the study; the changing Reynolds (Re_i) numbers with entry velocities were defined. Laminar and turbulent flow conditions were determined according to Reynolds numbers. At the equation; u_i represents the input velocity with respect to the reverse or forward flow, ρ represents the density of methane, μ represents the dynamic viscosity of methane, and D_H represents the hydraulic diameter.

In order to ensure the mesh independent solution and make sure that the model is running correctly, turbulence kinetic energy analysis was run for the various meshes. Turbulence kinetic energy did not change beyond the mesh number of 2 million. Therefore, the number of meshes used in the flow analyses was set to approximately 2.25 million.
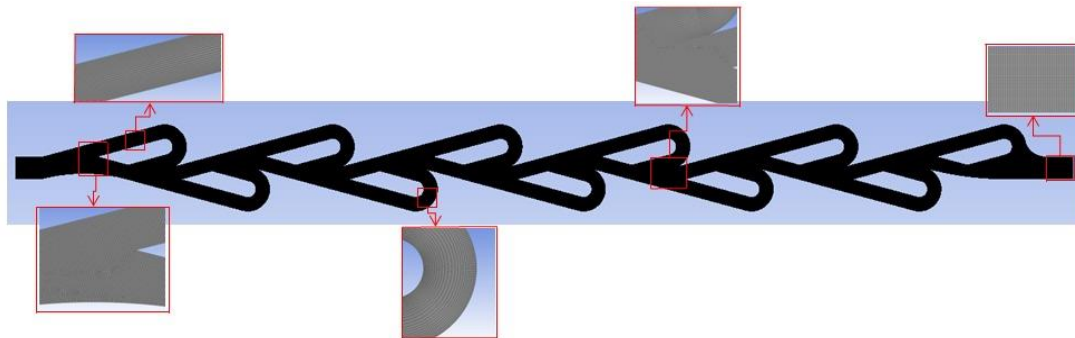

Figure 3. Tesla valve mesh structure.

The analyzes were performed using a 42 core parallel solver workstation. The Tesla valve mesh structure consists of regular rectangular mesh elements shown in Figure 3. The mesh model used has a total of 2249874 nodes, 2231746 cells, and 4481632 faces for simulations. The mesh structure was intensified in the boundary layer to capture the distinctive features of the flow process. Methane fuel was kept constant at 300 K for reverse and forward flows at all velocity inputs. Numerical solutions were gained for single-phase, incompressible Navier-Stokes equation sets with constant fluid properties. The analyzes for methane were carried out because the use of methane is widespread throughout the world, there is no study in this field for methane in the literature, and it is planned to examine the propagation of methane flame in the Tesla valve in the next study. For methane, whose flow behavior has been determined, the flame behavior in the Tesla valve will be examined in the next study.

$$\frac{\partial u_i}{\partial t} + \frac{\partial (u_i u_j)}{\partial x_j} = -\frac{1}{\rho}\frac{\partial P}{\partial x_i} + v\frac{\partial^2 u_i}{\partial x_i \partial x_j} \qquad \frac{\partial u_j}{\partial x_j} = 0 \tag{3}$$

In the model, an iterative solution was realized with flowing pressure-based separated solvent under continuous flow conditions. The k-ε-Realizable model was used to simulate the average flow properties under turbulent flow conditions, and laminar model was used to laminar flow conditions. The k-ε realizable turbulence model becomes significant for the formulation of events occurring in the turbulent flow region. Besides, in the k-ε realizable turbulence model, the formation of turbulent kinetic energy provided depending on the average velocity values. The k-ε realizable turbulencemodel differs from the standard k−ε model in two ways. Firstly; it contains a new formulation for the turbulent viscosity. The second difference is a new transport equation for the dissipation rate. These features give improved predictions for the spreading rate of jets, a superior ability to capture the mean flow of complex structures, and forward flows involving rotation, boundary layers under strong adverse pressure gradients, separation, and recirculation. Consequently; turbulence kinetic energy change, diodicity, inlet, and outlet pressure changes for the use of methane at different velocities in the Tesla valve were determined and the flow behavior was investigated in detail.

3. RESULTS

The effects of gas fluid motion at different velocities in an eleven-stage Tesla valve with a low angle configuration on diodicity were investigated numerically. The fluid motion behavior of methane gas between 1m/s-10 m/s in reverse and forward directions was investigated. The effect of methane sent to the Tesla valve at different velocities on the diode is shown in Figure 4. The diodicity up to Re = 4915 and the relationship between pressure drop and flow velocity has been investigated numerically. The diodicity dimished until the Reynolds number was Re <1966. In the transition region from laminar flow to turbulent flow ($1966 \leq$ Re≤ 2457), the diodicity swells in absolute. After Re> 2457, a decrease in diodicity was observed. The maximum diodicity was determined as 0.110 at Re = 2457 and the minimum diodicity as 0.046 at Re = 1966. It has been detected that the diodicity decreases in inverse proportion to the Reynolds number in both the laminar and turbulent regions, and it reaches from minimum to maximum diodicity in the transition from laminar to turbulent region.
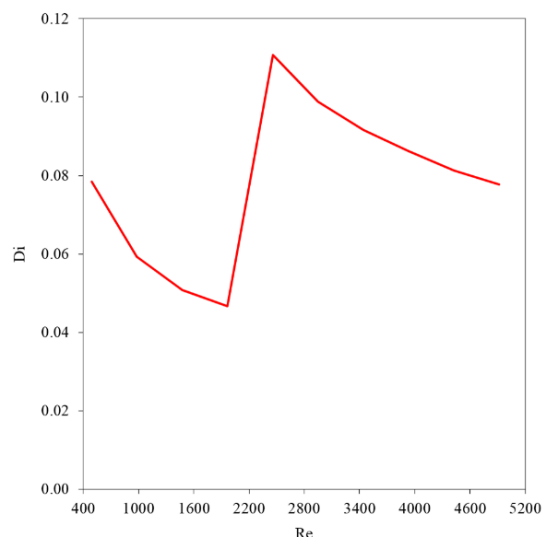
**Figure 4.** Di vs. Re trend.

The Tesla valve is a channel that changes resistance capability depending on the flow direction. The main flow line is divided into two and the flow collides when the flow comes from the reverse direction. In this case, the self-resistant flow appears inside the valve. Although there are no mechanical moving parts in the Tesla valve, the fluid behavior is restricted in the reverse flow or it is expected to slow down heavily because of its unique design. In forward flow, it is anticipated that the design will be able to flow without being exposed to any situation that may interfere with the flow.
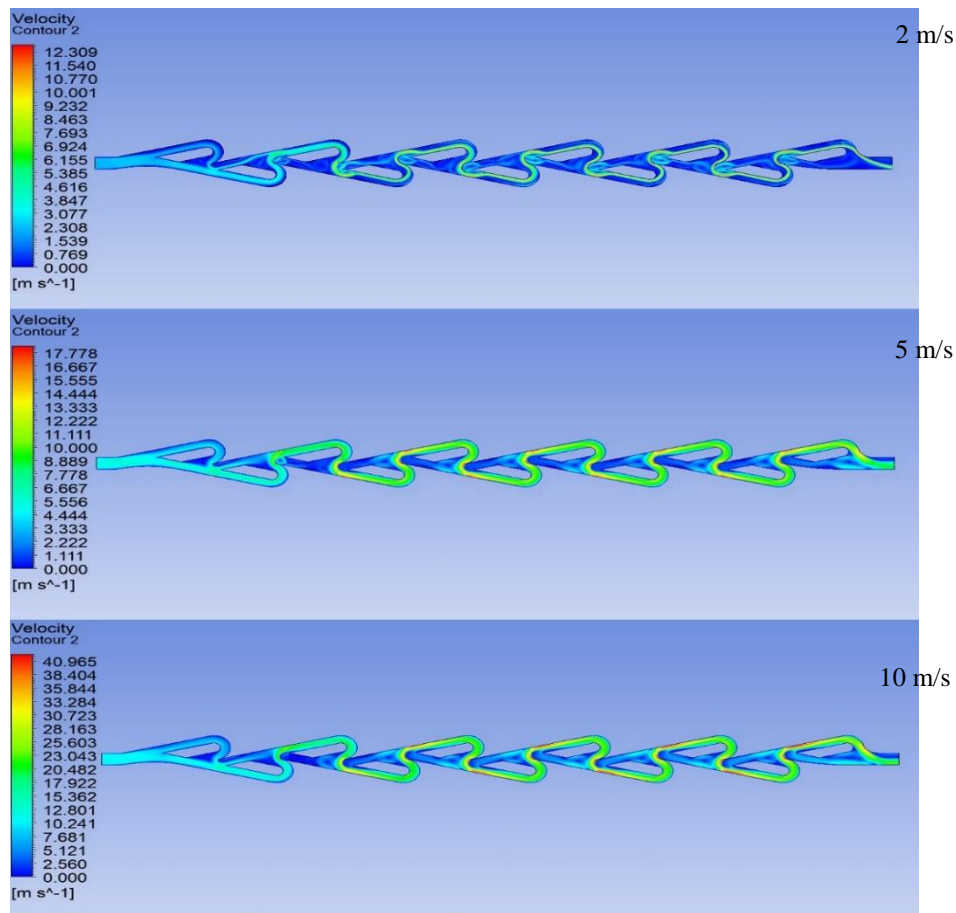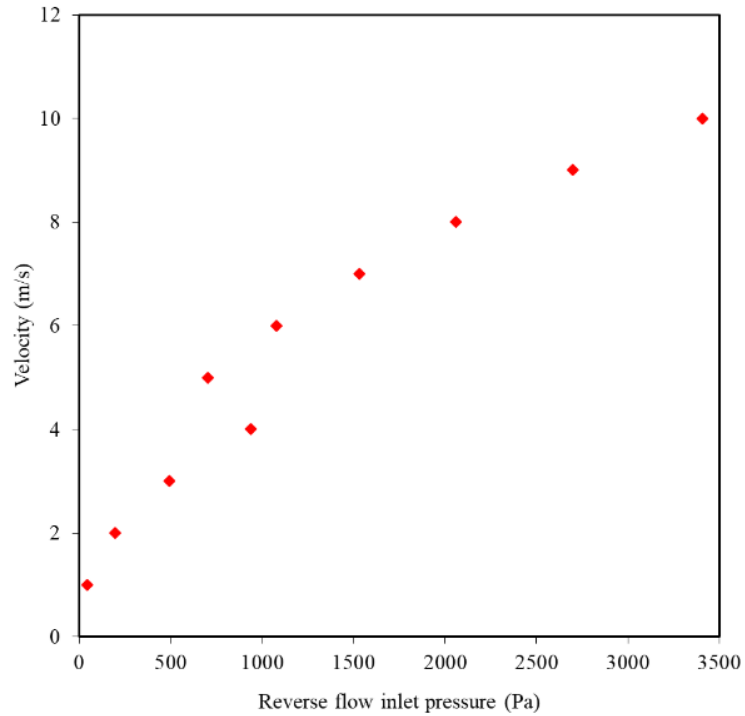

Figure 5. Reverse flow velocity.

The methane exhibits reverse flow from left to right as can be seen in Figure 5. In contour graphs, the display of the flow starts from the first step and progresses towards the fully developed flow up to the latest step and the red areas show where the fluid flows the fastest, while the blue areas represent the slowest flow. At the junction of discrete flow, vortices are occured, and these vortices increase the flow resistance, and it causes a gradual decrease in pressure. The eddies formed as a result of the collision are clearly visible on the contour graphs. The formed eddies direct most of the flow towards narrow wings. Therefore, a gradual decrease in pressure is provided.

In the study, it was observed that the lowest resistance was at a velocity of 1 m/s and the highest resistance occurred at a velocity of 10 m/s. In short, it is seen in reverse flow, when the resistance increases with the rise of velocity.
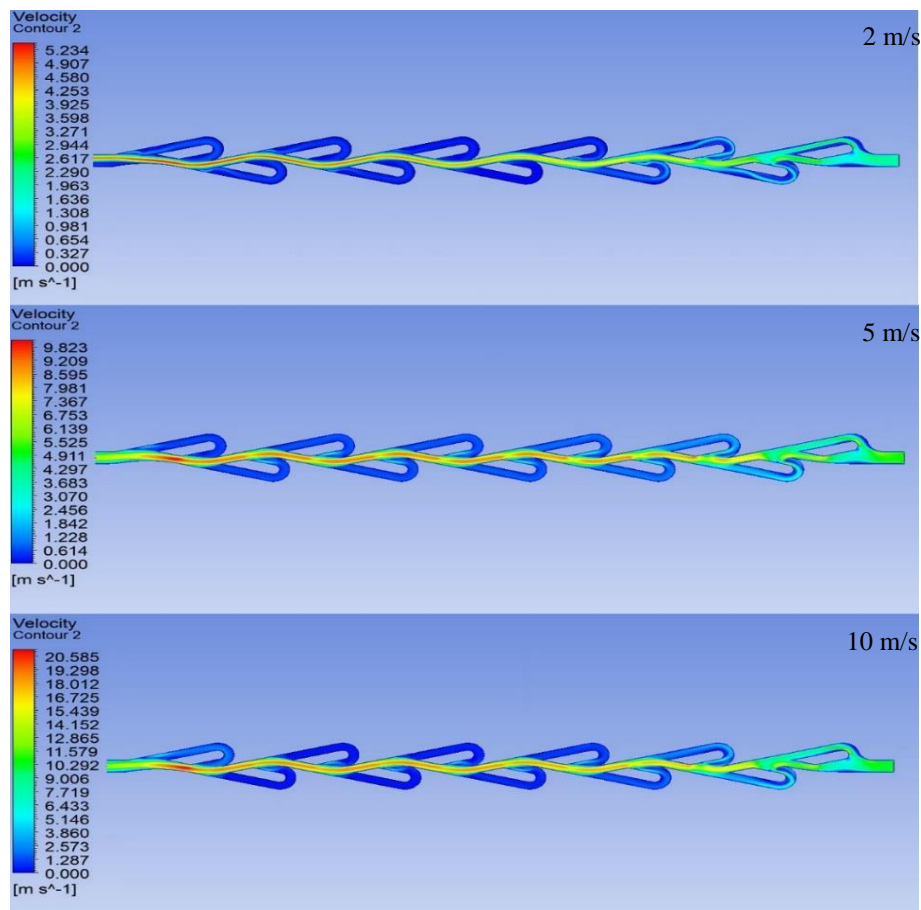

Figure 6. Flow velocity.

In Figure 6, the flow was sent from the opposite direction to the reverse flow. The contour graphs are also added as 2m/s, 5 m/s and 10 m/s respectively, from top to bottom. The evolution of forward flow from initial to fully developed flow is seen, and a few steps after the start of the flow, a smooth flow was created in the middle of the channel. The blue color was mostly observed in the wings, while the red color was observed in the regions where the flow moves from the middle to the forward. In this context, it is seen in the contour graph that the methane gas sent does not encounter much resistance along the channel.
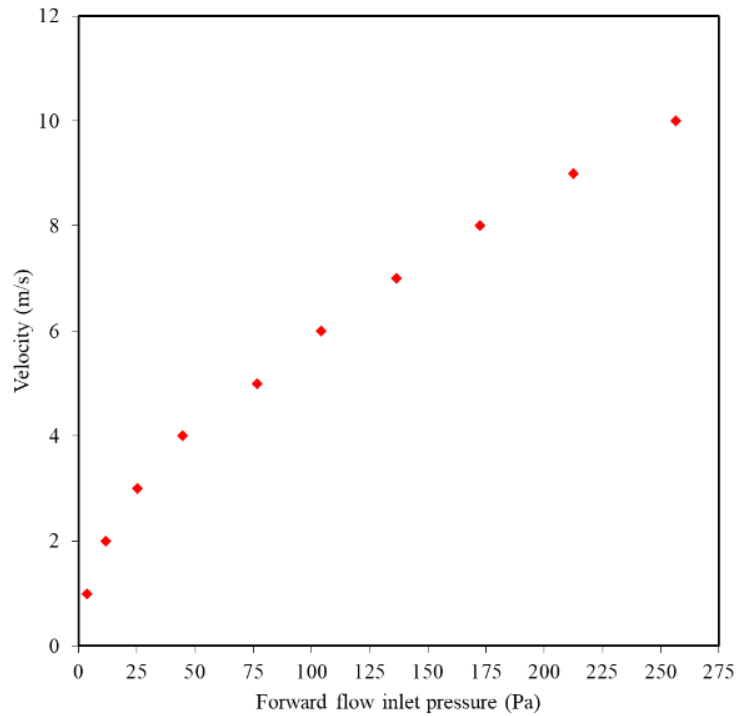
Figure 7. Velocity vs. Reverse flow inlet pressure.

The inlet pressure change depending on the velocity changes in reverse flow was given in Figure 7. The inlet pressure values shown in Figure 2 for reverse flow were obtained from line 1 data. The maximum inlet pressure was calculated at 3404 Pa when the inlet velocity was 10 m/s, and the minimum pressure value was calculated at 44 Pa at 1 m/s. It was observed that the pressure value increased with the increase of the velocity value in the laminar flow region. In the transition from laminar flow to turbulent flow region, it tended to instantaneous diminishes and then rises, similar to the diodicity chart. The trend of velocity-pressure variation in the turbulent flow region was similar to the change in the laminar region, showing a continuous upward trend.
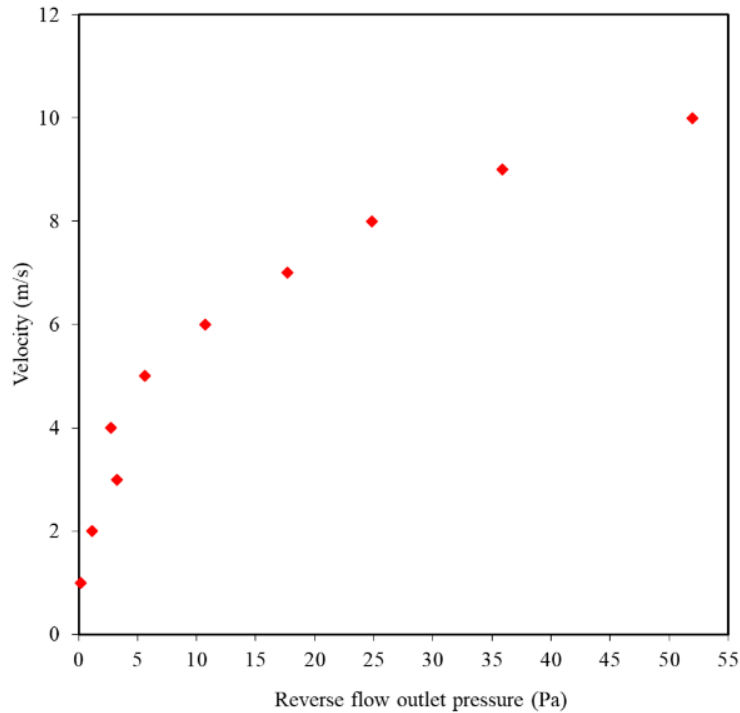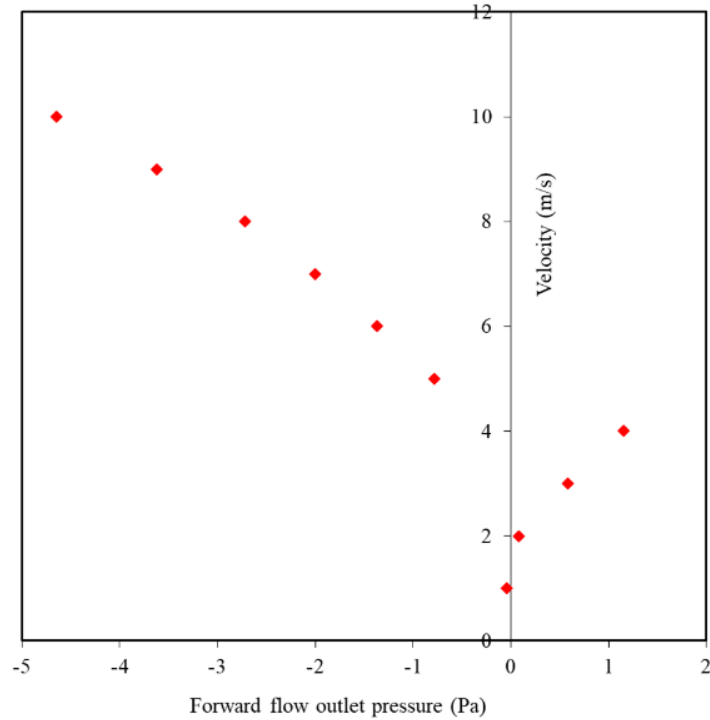
Figure 8. Velocity vs. Reverse flow outlet pressure.

Figure 8 shows that the output pressure change charts depending on the velocity changes in reverse flow. At the reverse flow, the outlet pressure of line 12 shown in Figure 2 was used. It is observed in Figure 8 that the maximum outlet pressure value increases depending on the velocity increase. While the maximum pressure is seen at 10 m/s velocity entry value, the lowest pressure is seen at the minimum velocity value of 1 m/s. On the other hand, the maximum pressure was about 51 Pa at an inlet velocity of 10 m/s, the minimum pressure value was calculated as 0.22 Pa in the analysis where the velocity was 1 m/s. Also, an exponential increment was observed in the laminar flow region, the exit pressure was continued to rise on the transition from the laminar region to the turbulent region.

Figure 9. Velocity vs. Forward flow inlet pressure.

The inlet pressure change charts depending on the velocity changes for forward flow were shown in Figure 9. The inlet pressure values shown in Figure 2 for forward flow are taken from the data read on the line 12 position When Figure 9 is examined, it is observed that the maximum inlet pressure value is 256 Pa at 10 m/s velocity. It was determined that the minimum pressure was 3.46 Pa at the lowest velocity, ie 1 m/s. It was observed that the inlet pressure rised because of the increase in velocity for the forward flow.

Figure 10. Velocity vs. Forward flow outlet pressure.

Figure 10 shows that the output pressure change charts depending on the forward flow velocity changes. Output pressure values shown in Figure 2 for forward flow are taken from line 1 data. It was observed that the outlet pressure rises during the laminar flow for the forward flow inlet pressure values. The maximum outlet pressure value was calculated as 1.15 Pa at 4 m/s. A sudden pressure drop was monitored during the transition from laminar flow to turbulent flow. Continuous decreasing pressure was detected from 5 m/s to 10 m/s in the turbulent region. There was a vacuum at the outlet pressure with the transition to turbulent flow. As the turbulent flow rate rises, the vacuum at the outlet pressure increases at the outlet pressure. It has been determined that the minimum pressure value is -4.645 Pa at 10 m/s. In this context, the laminar or turbulent flow regime in the Tesla valve affects the behavior of the flow.
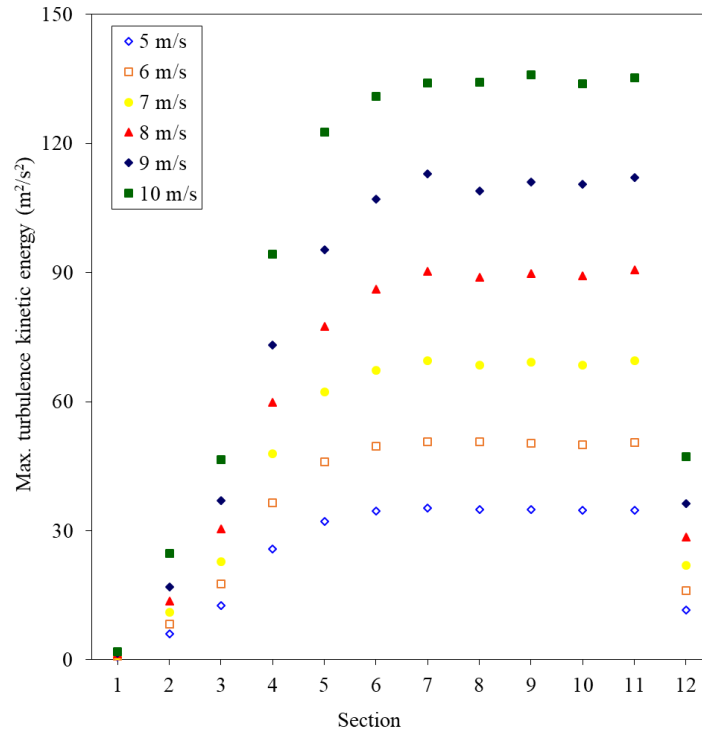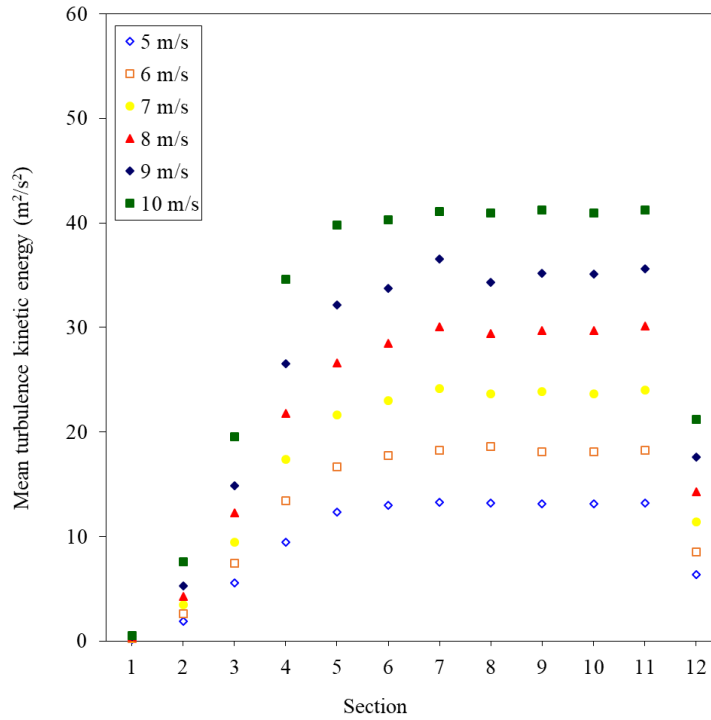
Figure 11. Maximum turbulence kinetic energy at reverse flow.

The maximum turbulence kinetic energy change depending on the velocity and position of the reverse flow was shown in Figure 11 and the flows displayed a linear increase in line 1, line 2, line 3, line 4 positions of the reverse flow depending on the turbulence kinetic energy. The flow development was considered to be completed after the line 5 position in reverse flow. It was detected that turbulence kinetic energy remained constant for all velocities after line 5. This trend is due to the tendency to slow down hereby collision of the flow. Turbulence kinetic energy kept constant after line 5 in reverse flow. Turbulence kinetic energies at line 6, line 7, line 8, line 9, line 10, and line 11 positions are almost the same. Turbulence kinetic energy has diminished at the line 12 point close to the exit.
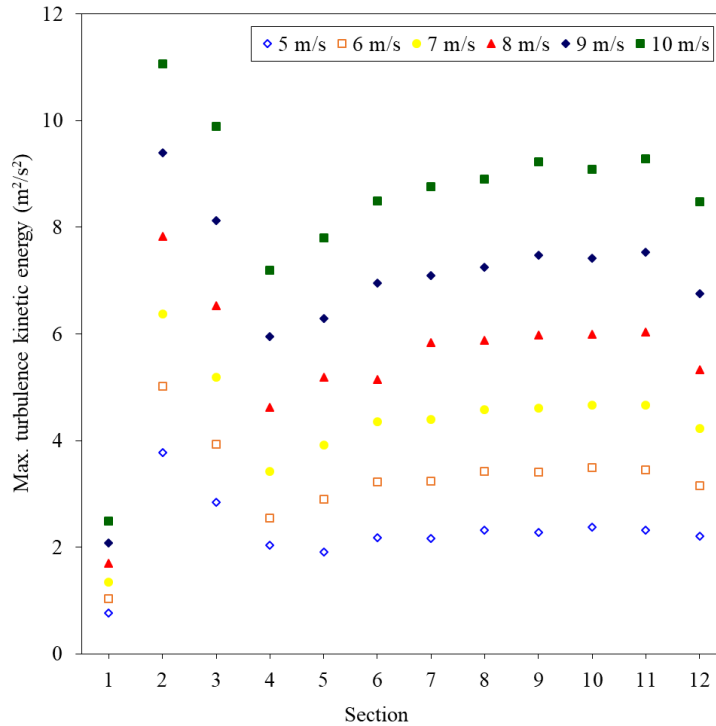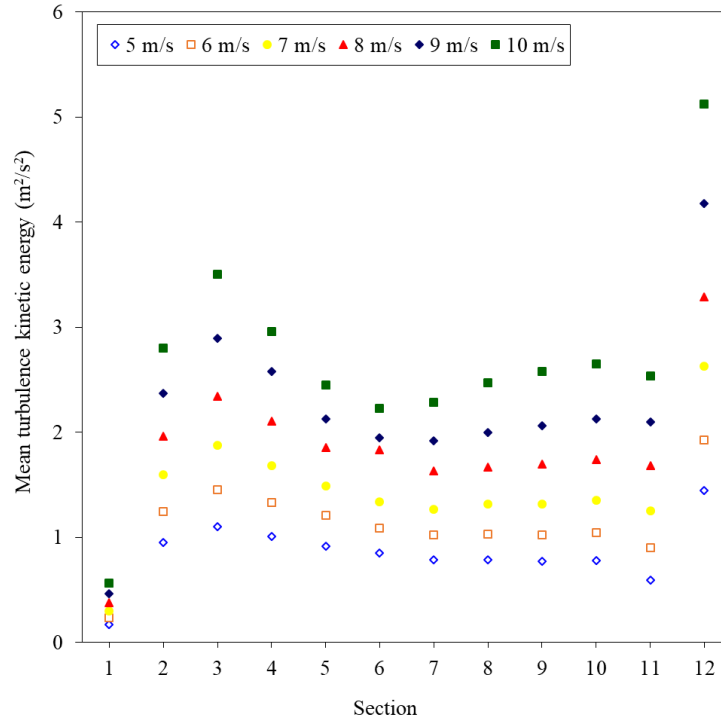
Figure 12. Maximum turbulence kinetic energy at forward flow.

Figure 12 shows that the maximum turbulence kinetic energy change depending on the velocity and position of the forward flow. The forward flow flows from line 12, which is the inlet port, to line 1. Since the flow from line 1 to line 2 is separated into two, turbulence kinetic energy has climbed the maximum points. Uniform flow towards line 3 was detected after line 2. Since an almost uniform flow forms after line 3, turbulence kinetic energy remained constant. The diminishes trend has been observed in the line 1 position, which is the outlet part.
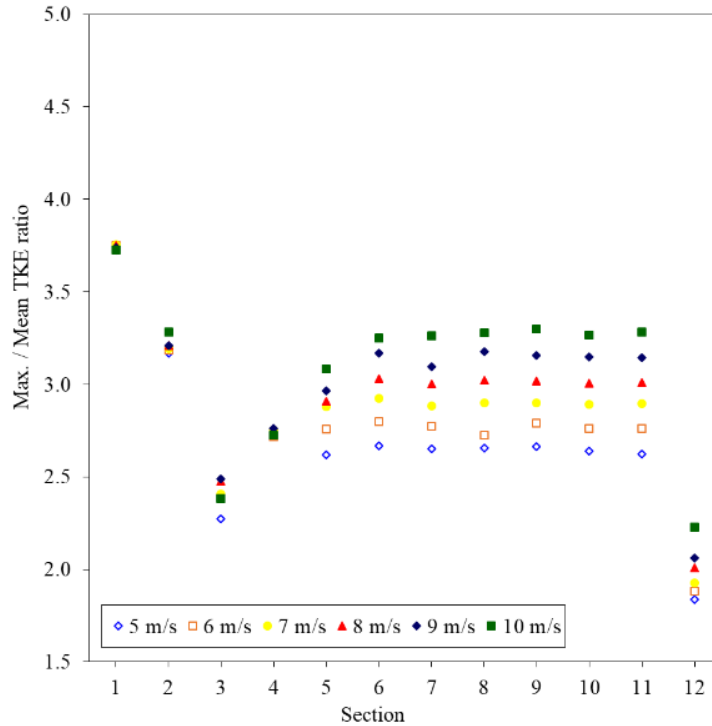
Figure 13. Mean turbulence kinetic energy at reverse flow.

The mean turbulence kinetic energy change depending on the velocity and position of the reverse flow was shown in Figure 13. Reverse flow average turbulence kinetic energy values are similar to Figure 11. The line 5 was observed an increase in both the maximum turbulence kinetic energy and the average kinetic energy. The flow that developed after line 5 showed almost uniform turbulence kinetic energy change in line 11. In the line 12, a decrease in turbulence kinetic energy change was observed while going towards the exit.
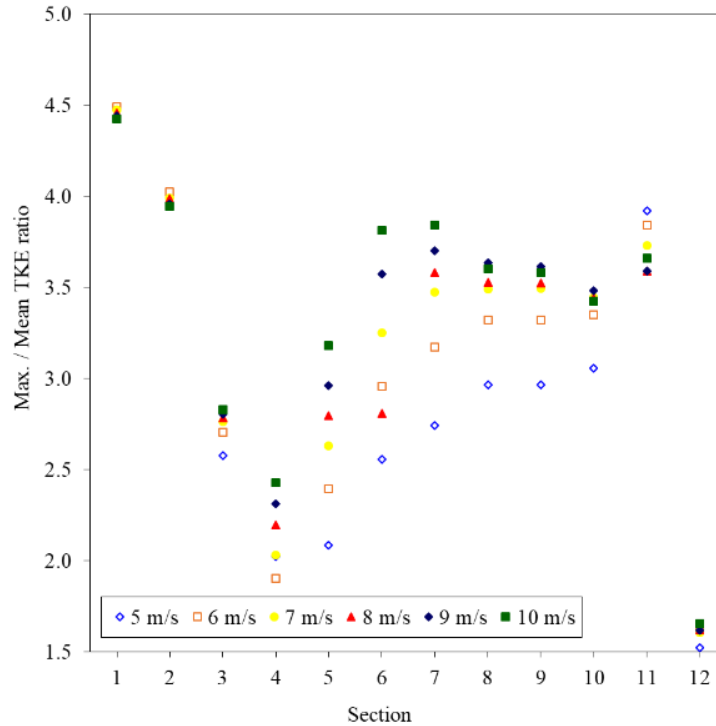
Figure 14. Mean turbulence kinetic energy at forward flow.

Figure 14 shows that the mean turbulence kinetic energy change depending on the velocity and position of the forward flow. Forward flow, average turbulence kinetic energy raised from line 12 to line 10. After line 10, the flow gathered in the center and continued on its way. The flows approaching a uniform structure after line 10 maintained constant turbulence kinetic energy at all velocities. The reason why the average turbulence kinetic energy climbs its maximum in line 1, which is the starting point, is thought to be due to the narrowing in the valve design. While there are sharp lines between positions in the chart of maximum turbulence kinetic energy change, it is seen a more gradual trend in the chart of average kinetic energy change.

Figure 15. Max. / Mean TKE ratio at reverse flow.

In Figure 15, the chart is made from the division of the maximum turbulence kinetic energy of the reverse flow by the mean turbulence kinetic energy. This chart aims to see the relationship between maximum turbulence kinetic energy and mean turbulence kinetic and the flow development is seen more clearly. There is the same ratio as the flow is not fully developed until it reaches the line 4 point for all velocities. After line 5, the rates change according to the velocity distributions with the development of the flow. Each flow from line 5 to line 11 position achieves a fixed-rate at its own velocity rate.

Figure 16. Max. / Mean TKE ratio at forward flow.

Figure 16 shows that the chart was obtained from the ratio of forward flow that maximum turbulence kinetic energy to mean turbulence kinetic energy. It has been observed that the ratios of maximum turbulence kinetic energy / mean turbulence kinetic energy at the inlet and outlet in forward flow are on coincident lines. Albeit these coincident lines are at different velocities, a fixed ratio is seen on the chart. The coincident lines at the entrance have begun to separate with the development of the flow at the entrance. The flow approaching the outlet leaves the system in coincident lines again. It has been observed that the rates at all velocities behave in the same direction as the direction changes along the flow. All positions for all velocities were parallel in directional motion.

4. CONCLUSION

In this study, the trends of the velocity of methane fuel in the specially designed Tesla valve have been investigated via computational fluid dynamics (CFD) methodology. Tesla valve structure with eleven flow control segments was used in the analyzes. The fluid motion behaviors in both directions were investigated for laminar and turbulent types. Two different directional analyzes were carried out as flow directions reverse and forward flow. Inlet and outlet pressures for flow from both directions were investigated separately. The diodicity up to Re = 4915 and the relationship between pressure drop and flow velocity has been investigated numerically. When the Reynolds number is Re <1966, the diodicity was decreased in the analyzes. In the transition region from laminar flow to turbulent flow (1966 ≤ Re ≤ 2457) the diodicity was risen in absolute. In the case of Re> 2457, a reduction in

diodicity was detected. The maximum diodicity was observed at 0.110 at Re = 2457 and the minimum diodicity was detected at Re = 1966 at 0.046.

It was seen that vortices occurred with the mutual collision of the flow for reverse flow. For the inlet pressure, it was observed that the pressure value soared up with the increase of the velocity in the laminar flow region. There was a partial dwell and then an increase in the transition from laminar flow to turbulent flow region. In the turbulent flow region, the velocity-pressure change has steadily swelled. While an exponential throw is detected in the laminar flow region for the outlet pressure, the pressure continued to increase in the transition from the laminar region to the turbulent region. A linear increase was seen in the maximum turbulence kinetic energy until the fully developed flow and after line 5, the flow was continued on its way, completing its development. Afterwards, it was seen that the turbulence kinetic energy remained almost the same for all velocities. A decrease in turbulence kinetic energy was observed at the line 12 point, which is close to the exit point. The average turbulence kinetic energy is similar to the maximum turbulence kinetic energy chart. In order to see the relation between maximum turbulence kinetic energy and average turbulence kinetic energy, a chart was created by dividing the maximum turbulence kinetic energy by the average turbulence kinetic energy. It remained at a constant rate after the development of flow until line 5. After that, the rates were changed according to the velocity distributions with the development of the flow.

It was seen that the flow continues over the main channel at pass the second stage in forward flow. Also, it was seen that the inlet pressure rise in direct proportion to the velocity in forward flow. The outlet pressure soared up with the increase of laminar flow, while the vacuum was observed in the turbulent flow. The vacuum trend was seen soared up even more as the velocity increased in the turbulent flow. The maximum turbulence kinetic energy has reached the maximum point since it flows in two directions in the first stage. Afterward, it turned towards a constant flow. There was a diminished in the exit positions. The average turbulence kinetic energy chart is similar to the maximum turbulence kinetic energy chart for analysis. Forward flow average turbulence kinetic energy increased from Line 12 to Line 10. After Line 10, the flow gathered in the center and continued on its way. Flows approaching a uniform state after Line 10 maintained constant turbulence kinetic energy at all velocities. The reason for the average turbulence kinetic energy to reach its maximum in line 1, which is the starting point, is thought to be because of the narrowing in the design of the valve. In the chart of maximum turbulence kinetic energy change, the lines between positions are sharp, while the average kinetic energy change chart is seen more gradually. The chart, which consists of the division of the maximum turbulence kinetic energy by the average turbulence kinetic energy, showed a development trend similar to the reverse flow chart.

ACKNOWLEDGEMENT

REFERENCES

[1] Tesla, N., (1920), Valvular Conduit, U.S. Patent no. 1, 329-559.

[2] Stemme, E. and Stemme, G., (1993), A valveless diffuser/nozzle-based fluid pump, Sensors and Actuators A: physical, 39, 159-167.

[3] Gerlach, T., (1998), Microdiffusers as dynamic passive valves for micropump applications, Sensors and Actuators A: Physical, 69, 181-191.

[4] Tsai, C.H., Lin, C.H., Fu, L.M. and Chen H.C., (2012), High-performance microfluidic rectifier based on sudden expansion channel with embedded block structure, Biomicrofluidics, 6, 24108-241089.

[5] Fadl, A., Zhang, Z., Geller, S., Tölke, J., Krafczyk, M. and Meyer, D., (2009), The effect of the microfluidic diodicity on the efficiency of valve-less rectification micropumps using Lattice Boltzmann Method, Microsystem Technologies, 15, 1379-1387.

[6] Truong, T. Q. and Nguyen, N.T., (2003), Simulation and optimization of tesla valves, Nanotech Nanotechnology Conference and Trade Show, San Francisco,178-181.

[7] Forster, F. K., Bardell, R.L., Afromowitz, M.A. and Sharma, N.R., (1995), Design, fabrication and testing of fixed-valve micro-pumps, Asme-Publications-Fed, 234,39-44.

[8] Zhang, S., Winoto, S.H. and Low, H.T., (2007), Performance simulations of Tesla microfluidic valves, International Conference on Integration and Commercialization of Micro and Nanosystems, Sanya, China, The American Society of Mechanical Engineers, New York,15-19.

[9] Gamboa, A.R., Morris, C. J. and Forster, F.K., (2005), Improvements in fixed-valve micropump performance through shape optimization of valves, 127, 339-346.

[10] Thompson, S.M., Jamal, T., Paudel, B. J. and Walters, K.D., (2013), Transitional and turbulent flow modeling in a tesla valve, ASME International Mechanical Engineering Congress and Exposition, American Society of Mechanical Engineers 56321.

[11] Mohammadzadeh, K., Kolahdouz, E. M., Shirani, E. and Shafii, M. B., (2013), Numerical Investigation on the effect of the size and number of stages on the Tesla microvalve efficiency, Journal of Mechanics, 29, 527-534.

[12] Porwal, P.R., Thompson, S. M. and Walterss, K.D. & Jamal, T., (2018), Heat transfer and fluid flow characteristics in multistaged Tesla valves, Numerical Heat Transfer, Part A: Applications, 73, 347-365.

[13] Thompson, S. M., Ma, H. and Wilson, C., (2011), Investigation of a flat-plate oscillating heat pipe with Tesla-type check valves, Experimental Thermal and Fluid Science, 35,1265-1273.

[14] Bardell, R. L., (2000), The diodicity mechanism of tesla-type no-moving-parts valves, Ph.D. dissertation, University of Washington, Seattle, WA.

[15] Qian, J.Y., Chen, M.R. and Liu, X.L.& Jin, Z. J., (2019), A numerical investigation of the flow of nanofluids through a micro Tesla valve, Journal of Zhejiang University-SCIENCE A, 20, 50-60.

[16] Jin, Z.J., Gao, Z.X., Chen, M.R. and Qian, J.Y., (2018), Parametric study on Tesla valve with reverse flow for hydrogen decompression, International Journal of Hydrogen Energy, 43, 8888-8896.

[17] Wang, C.T., Chen, Y.M., Hong, P.A. and Wang, Y.T., (2014), Tesla valves in micromixers, International Journal of Chemical Reactor Engineering 1.open-issue.